Growth Kinetics and Metastability of Monodisperse Tetraoctylammonium Bromide Capped Gold Nanocrystals

Aaron E. Saunders, Michael B. Sigman Jr., and Brian A. Korgel*

Department of Chemical Engineering, Texas Materials Institute and Center for Nano- and Molecular Science and Technology, The University of Texas, Austin, Texas 78712-1062

Received: August 4, 2003; In Final Form: October 24, 2003

Small-angle X-ray scattering (SAXS) was used to measure the time-dependent evolution of the size and size distribution of tetraoctylammonium-stabilized gold nanocrystals formed by arrested precipitation. The initial growth mechanism was varied by controlling the addition of reducing agent to the ionic gold precursor solution. Slow addition gives high Au^0 monomer supersaturation and provides discrete nucleation and growth events and a narrowing of the particle size distribution over short reaction times. Rapid addition of reducing agent leads to broad initial particle size distributions that begin to narrow only after the first few hours of the reaction. After 24 h, the nanocrystals grow to 52 Å in diameter with a very narrow size distribution regardless of the initial growth kinetics. Analysis of the reaction and transport rates reveal that nanocrystal growth is limited by the surface reaction rate of monomer addition to the crystal surface. The final size appears to be thermodynamically metastable, with the system free energy, which includes the gold surface tension and the tetraoctylammonium binding energy, reaching a local minimum. Nanocrystal size is also found to vary inversely with the binding strength of the capping ligand present during growth, allowing the mean particle diameter to be tuned to between 1.7 and 5.2 nm.

Introduction

The use and study of colloidal gold particles has a long history. Gold colloids have been used as colorants in glazes, glasses, and paints from at least the time of the Roman Empire,[1] and their chemical and optical properties have been studied since the work of Faraday[2] and Mie[3] in the mid 1800s and early 1900s. A recent "resurgence" in colloidal gold nanocrystal research has been driven primarily by the ability to synthesize organic monolayer-coated nanocrystals with diameters smaller than 6 nm and their newfound technological uses in catalysis,[4,5] biology,[6] and the fabrication of novel nanoscopic materials.[7−9] These technological applications depend on the ability to produce large quantities of nanocrystals with controlled size and size distributions.

Arrested precipitation has been a successful synthetic method for the formation of metal and semiconducting nanocrystals. This approach utilizes organic ligands that adsorb to the particle surface to prevent their aggregation and stabilize their size. Although successful in producing size-monodisperse nanocrystals less than 10 nm in diameter, the growth mechanisms are not well understood because limited data exist on the time-dependent evolution of the particle size and size distribution.

Here, we present small-angle X-ray scattering (SAXS) data for hydrophobic gold nanocrystals produced by a two-phase arrested precipitation as a function of reaction time. Information about the size distribution can be determined from SAXS, providing a snapshot of how the size and polydispersity evolve during the synthesis. As shown below, the initial particle size and size distribution depend on the initial concentration of gold precursor and the method used to carry out the reduction. However, despite qualitative differences in the mechanism for particle formation at early reaction times, the size and size distribution evolve to reach a final diameter of 5.2 nm (average) and a standard deviation of 0.64 nm (12%) without a size selective separation *regardless of the initial growth conditions*. We present a model explaining the interplay between the size-dependent gold surface energy and the ligand−surface bond energy and its effect on the final nanocrystal size.

* Author to whom correspondence should be addressed. Phone: (512) 471-5633. Fax: (512) 471-7060. E-mail: korgel@mail.che.utexas.edu.

Experimental Section

All chemicals were used as received and all water was doubly distilled and deionized. Hydrogen tetrachloroaurate (III) trihydrate ($HAuCl_4 \cdot 3H_2O$), tetraoctylammonium bromide ($((C_8H_{17})_4NBr$), tetraoctylphosphonium bromide ($((C_8H_{17})_4PBr$), sodium borohydride ($NaBH_4$), octanethiol ($C_8H_{17}SH$), and dodecanethiol ($C_{12}H_{25}SH$) were purchased from Aldrich Chemical Company. Toluene was obtained from Fisher Scientific.

Nanocrystal Synthesis. Gold nanocrystals were synthesized using a modification of established two-phase arrested precipitation methods.[10,11] Tetraoctylammonium bromide (TOAB) was used as both a phase transfer catalyst and a capping ligand. Nanocrystals were synthesized by adjusting the initial precursor concentration and controlling the addition of reducing agent (see Table 1 for a summary of reaction conditions).

(i) Separate Nucleation and Growth. In a typical experiment, 3.0 mL of 0.03 M aqueous tetrachloroaurate (0.09 mmol) solution was combined with 50 mL of toluene containing 1.0 g (1.8 mmol) of TOAB. Complete transfer of the gold ions from the aqueous phase to the organic phase occurred after 30 min of vigorous stirring, at which point the aqueous phase was separated and discarded. The gold precursor concentration in the organic phase was then 1.8 mM. The organic solution was stirred vigorously while adding the aqueous reducing solution

10.1021/jp036272g CCC: $27.50
Published on Web 12/09/2003

TABLE 1: Comparison of Reaction Conditions Used for Separated and Concurrent Nucleation and Growth Stages

	separate nucleation and growth	concurrent nucleation and growth
rate of addition of reducing agent	dropwise until color change	immediate
initial gold concentration in organic phase, $[AuCl_4^-]_0$	1.8 mM	38.6 mM
phase transfer catalyst/Au molar ratio	20:1	5:1
sodium borohydride/Au molar ratio	12:1	14:1

(2.5 mL of 0.4 M $NaBH_4$ (1 mmol)) by pipet at a rate of one drop ($\approx$30 μL) every 15 s; the color of the organic phase was carefully monitored as it gradually changed from orange to yellow to clear. The solution turned clear after approximately 20 drops (0.6 mL). An additional drop of reducing solution turned the organic solution a very light brown tint, at which point the remainder of the reducing solution was injected. The resulting nanocrystal dispersion was stirred for 24 h, at which point 200 μL (0.835 mmol) of dodecanethiol, which is a much stronger capping ligand than TOAB, was added to passivate the nanocrystal surface and prevent further growth. The nanocrystal dispersion was stirred for 1 h and then purified as described below.

(ii) Concurrent Nucleation and Growth. Here, the gold chloride ions initially present in 15 mL of DI-H_2O (0.064 M, 0.965 mmol $HAuCl_4 \cdot 3H_2O$) were transferred into 25 mL of toluene containing 2.7 g (4.9 mmol) of phase transfer catalyst. Transfer of the gold ions into the organic phase was complete after 30 min of stirring. The aqueous phase was then separated and discarded. The gold ion concentration in the toluene phase was 38.6 mM. Reducing agent (30 mL of 0.44 M $NaBH_4$ in DI-H_2O (13.2 mmol)) was added to the organic solution under vigorous stirring. The solution instantly appeared dark brown and gradually became red over the course of several hours. After stirring for 24 h, 240 μL (1.0 mmol) of dodecanethiol was added to the mixture, and then it was stirred for an additional hour.

(iii) Phosphine and Thiol-Stabilized Nanocrystal Growth. The binding strength of the capping ligand present during nanocrystal growth was also investigated. The reactions were carried out using similar conditions as those described above in the separate nucleation and growth section. Here, 0.09 mmol of gold ions was transferred into 50 mL of toluene. In one experiment the phase transfer catalyst was 1.8 mmol of tetraoctylphosphonium bromide, which also acted as the capping ligand during growth. In a second experiment the phase transfer catalyst was 1.8 mmol of tetraoctylammonium bromide; however, the organic phase also contained 1.8 mmol of octanethiol. The binding strength of the thiol is much stronger than the amine; hence, the thiol displaces the amine and acts as the protecting ligand during growth. After phase transfer was complete and the organic phase had been separated, 1 mmol of $NaBH_4$ (in 2.5 mL of DI-H_2O) was added immediately while stirring. The reactions were allowed to proceed for 24 h. Although the phosphine-capped gold nanocrystals appeared to be well stabilized in solution, 0.835 mmol of dodecanethiol was added to the solution to ensure particle stability during cleaning and characterization.

After the nanocrystal surfaces were passivated with the alkanethiol ligands, the aqueous phase was removed and discarded, leaving the nanocrystal rich toluene phase. Ethanol was added in excess to the toluene mixture as an antisolvent, and the nanocrystals were precipitated by centrifugation. The nanoparticles coated the sides of the centrifuge tubes allowing the supernatant, containing excess phase transfer catalyst, thiol, and reaction byproducts, to be discarded. The nanocrystals could then be dispersed into toluene and other organic solvents for analysis.

Nanocrystal Characterization. The nanocrystal size and size distributions were determined at various reaction times by withdrawing 1 mL aliquots of the nanocrystal dispersion. The nanocrystals were stabilized and growth was quenched immediately by adding excess dodecanethiol (approximately a 300:1 thiol/gold molar ratio). The samples were then cleaned as described above prior to characterization by transmission electron microscopy (TEM), high-resolution scanning electron microscopy (HRSEM), and small-angle X-ray scattering (SAXS).

TEM images were acquired on a Phillips EM280 microscope with a 4.5 Å point-to-point resolution operated with an 80 kV accelerating voltage. Nanocrystals were deposited from a dilute toluene solution onto 200 mesh carbon-coated copper TEM grids (Electron Microscopy Sciences). HRSEM imaging was performed on a LEO 1530 SEM equipped with a GEMINI field emission column with a thermal field emitter. HRSEM samples were prepared by drop casting concentrated nanocrystal dispersions on a glassy carbon substrate. SAXS was performed using a rotating copper-anode generator (Bruker Nonius) operated at 3.0 kW. Scattered photons were collected on a multiwire gas-filled detector (Molecular Metrology, Inc.). The scattering angle was calibrated using a silver behenate ($CH_3(CH_2)_{20}COOAg$) standard and all experimental data were corrected for background scattering and sample absorption. SAXS measurements were acquired from both dilute toluene dispersions and nanocrystal films drop cast on Kapton substrates.

Results and Discussion

Time-Dependent Evolution of the Nanocrystal Size and Size Distribution. The gold nanocrystal size and size distribution were measured using SAXS. TEM was also used as a complimentary technique; however, this method must be used with care as it generally does not provide an accurate determination of the true size distribution of the sample because it limits observations to fields of only hundreds of nanocrystals. SAXS investigates more statistically relevant ensembles of as many as 10^{10} particles in the scattering volume and provides a very sensitive probe to subtle differences in size and shape. Figure 1a shows representative SAXS data for nanocrystals collected at different reaction times redispersed in toluene. The scattered intensity, $I(q)$, oscillates with increasing wave vector $|\boldsymbol{q}| = q = 4\pi/\lambda \sin(\theta)$ (λ is the wavelength (0.154 nm) and 2θ is the scattering angle). These oscillations relate to the nanocrystal size; because q is inversely proportional to a characteristic length in the system, $q = 2\pi/l$, inspection of the data reveals that the nanocrystal diameter increases with longer reaction time.

SAXS provides a quantitative determination of the nanocrystal radius R, size distribution, interparticle interactions, and nanocrystal order. $I(q)$ depends on scattering contributions from the individual nanocrystals, which are accounted for by the shape factor $P(qR)$, and multiparticle scattering effects that are accounted for in the structure factor $S(q)$. In fact, only the shape and structure factors are needed to account for the q-dependence of the scattered intensity: $I(q) \propto P(qR)S(q)$. In dilute dispersions, nanocrystals scatter as an ensemble of independent noninteracting particles with $S(q) = 1$. Because $I(q) \propto P(qR)$ under these conditions, $P(qR)$ can be measured directly to determine the size and size distribution using the appropriate shape factor,[12−15]

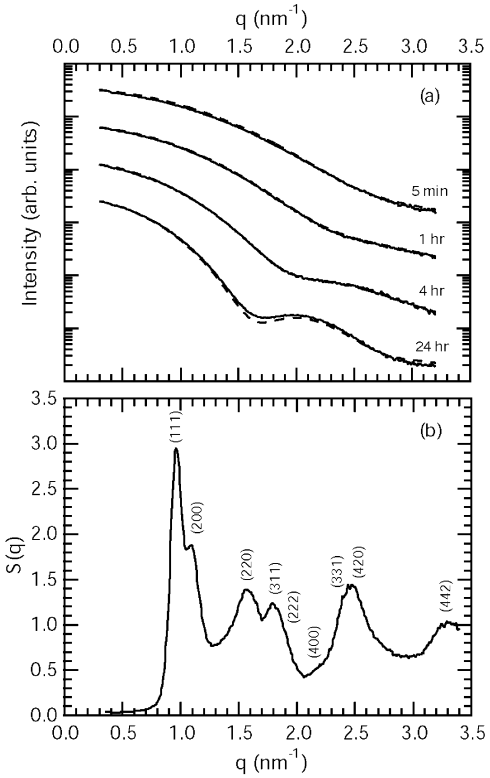

Figure 1. (a) Small-angle X-ray scattering (SAXS) data from dispersions of nanocrystals removed from the reaction mixture at different times. (b) The structure factor, *S(q)*, for a nanocrystal thin film determined through small-angle X-ray diffraction. The peaks in the structure factor can be indexed to a face-centered cubic lattice, with a lattice parameter of $a = 11.3$ nm.

which for a solid sphere is[16,17]

$$P(qR) = \left[3\frac{\sin(qR) - qR\cos(qR)}{(qR)^3}\right]^2 \qquad (1)$$

The polydispersity is readily accounted for since $I(q) \propto \int N(R) P(qR) R^6 \, dR$,[17] where *N(R)* is the number fraction of nanocrystals of radius *R* in the ensemble. The shape of the size distribution must be assumed in order to calculate the intensity. Here we assume a Gaussian size distribution with average radius R_{avg} and standard deviation σ:

$$N(R) = \frac{1}{\sigma\sqrt{2\pi}} \exp\left[\frac{-(R - R_{avg})^2}{2\sigma^2}\right] \qquad (2)$$

Figure 1a shows typical curve fits used to extract R_{avg} and σ from the SAXS measurements. The sharpness of the oscillations in $I(q)$ depends sensitively on the nanocrystal size distribution. A reasonably broad size distribution ($\sigma/R_{avg} \gtrsim 30\%$) smears the oscillations completely. The data in Figure 1a show that the nanocrystal size distribution narrows with increased reaction time.

The values of R_{avg} and σ determined from SAXS for the growth experiments are compiled in Figure 2. The data show that the initial growth kinetics depend on the how the reducing agent is added to the reaction mixture. Immediate addition of reducing agent produces 3.0 nm diameter nanocrystals with a broad size distribution ($\sigma/R_{avg} = 27\%$) that does not change during the first 2 h of the reaction. In comparison, controlled nucleation and growth through careful addition of reducing agent

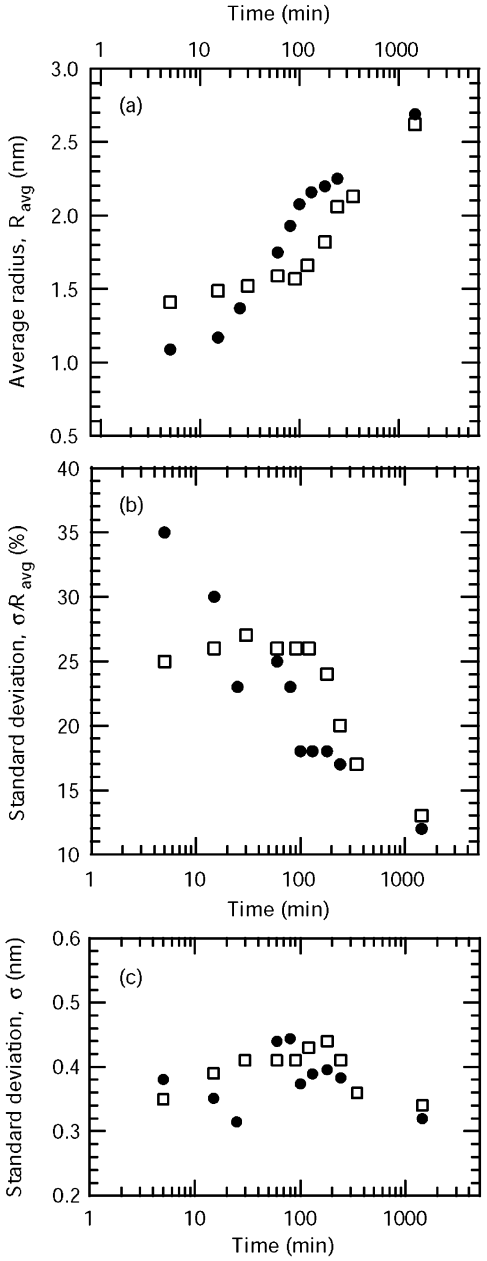

Figure 2. (a) Average nanocrystal size, (b) standard deviation as a percentage of the average size, and (c) standard deviation in nanometers as a function of reaction time, determined by small-angle X-ray scattering, for separate nucleation and growth (●) and concurrent nucleation and growth (□).

produces nanocrystals that evolve from 2.0 to 4.2 nm in diameter with σ/R_{avg} decreasing from 34% to 17% during the first 2 h. The radius rapidly increases during the first 90 min before the growth rate slows. The polydispersity also drops quickly in the first 90 min and then slowly decreases over the remainder of the reaction time.

Surprisingly, the size distribution narrows significantly at longer reaction time *independent of the initial growth kinetics*. After 24 h, the nanocrystals become quite monodisperse ($\sigma/R_{avg} \approx 12\%$) with an average particle diameter of 5.2 nm. Several reactions were performed with different precursor concentrations and rates of reducing agent addition. In all cases, the average mean nanocrystal diameter was 5.2 nm with an average standard deviation of 0.64 nm (12%) as determined by SAXS. Therefore, this size appears to represent a metastable size for tetraoctylammonium bromide capped Au nanocrystals.

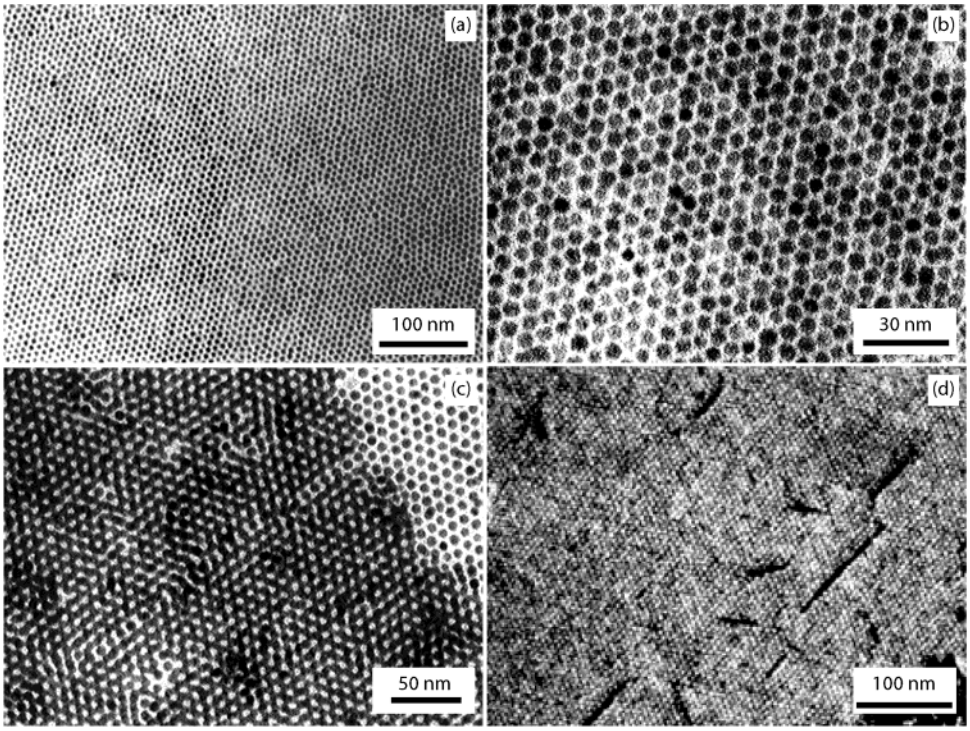

Figure 3. Dodecanethiol-capped gold nanocrystals after 24 h of growth. TEM images of (a,b) nanocrystal monolayers and (c) a bilayer of particles in an fcc arrangement. (d) HRSEM image of a nanocrystal thin film. The samples in (a) and (d) were synthesized by adding the reducing agent dropwise; (b) and (c) are from reactions where the reducing agent was added all at once.

Figure 3 shows TEM and HRSEM images obtained from nanocrystals synthesized using both reaction methods. Extensive monolayers of hexagonally close-packed nanocrystals were observed, as well as regions of ordered three-dimensional packing. Figure 3c shows a bilayer of nanocrystals arranged into two planes of a face-centered cubic (fcc) lattice. Figure 1b shows SAXS data for superlattices formed by drop casting these nanocrystals onto Kapton substrates. The diffraction peaks index to an fcc superlattice, as expected for relatively monodisperse nanocrystals in this size range.[13,18]

Particle Growth Kinetics. The initial growth kinetics can be explained within the theoretical framework proposed by LaMer and Dinegar,[19,20] in which the polydispersity of the prepared colloid is determined by homogeneous nucleation of a supersaturated solution and subsequent growth. LaMer originally proposed that monodisperse colloids could be prepared by supersaturating a solution with monomer. Homogeneous nucleation occurs when the concentration exceeds a "critical limiting supersaturation," which drops the monomer concentration below the supersaturation concentration. Provided that aggregation and further nucleation do not occur, the remaining monomer deposits uniformly onto existing nuclei to give monodisperse colloids.

Separation of nucleation and growth, as is commonly done in the preparation of semiconductor and magnetic quantum dots,[21−23] was accomplished by controlled addition of reducing agent under high TOAB/Au ratios with careful monitoring of the solution color. The deep orange color of the initial organic phase results from the charge-transfer complex between the gold (III) chloride ions ($AuCl_4^-$) and the tetraoctylammonium molecules. Slow addition of $NaBH_4$(aq) reduces a portion of the $AuCl_4^-$ ions to atomic Au^0 and possibly subnanometer clusters of gold $(Au^0)_m$. As reducing agent is added, the solution color fades from dark orange to yellow and finally becomes clear after approximately 10% of the reducing solution has been added. The color change results from the formation of small gold clusters and atoms that do not absorb visible light.[24,25] Further $NaBH_4$(aq) addition produces a very slight brown color, characteristic of gold nanoparticles with core diameters between 1 and 2 nm.[11] TOAB and other quaternary ammonium bromide salts act as a weak stabilizing ligand for gold nanocrystals,[25,26] and here the relatively dilute conditions and large TOAB/Au ratio (20:1) limit monomer aggregation and particle growth. Much lower TOAB/Au ratios of 1:1 in the reaction mixture were also explored and did not suppress particle aggregation, making it impossible to achieve high monomer supersaturation under these conditions. Injecting the remaining $NaBH_4$(aq) solution converts the residual gold ions to Au^0 and promotes homogeneous nucleation. The solution immediately changes from clear to a dark brown color, indicating rapid nanocrystal growth. Although further homogeneous nucleation could potentially occur at the water/organic interface, heterogeneous condensation of Au^0 atoms onto existing nuclei is much more energetically favorable, and the mean particle size rapidly increases and the size distribution narrows (Figure 2).[20,27]

Under conditions of higher gold concentration, lower TOAB/Au ratio, and immediate uncontrolled addition of excess reducing agent, the gold nanocrystals exhibit initial growth kinetics qualitatively distinct from those observed with controlled addition of reducing agent. As shown in Figure 2, the nanocrystals reach a size of 3.0 nm in diameter with a broad size distribution that does not evolve during the first 120 min of the reaction. Under these highly concentrated conditions, nucleation and growth occurs simultaneously with the Au^0 monomer production rate at the toluene/water interface. The immediate addition of reducing agent causes a large initial gold monomer supersaturation at the solvent/water interface. Nucleation relieves the supersaturation localized at the interface; however, the relatively high gold ion concentration promotes further reduction at the interface as the nuclei diffuse into the bulk of the organic solution. This simultaneous nucleation and growth process leads to a high degree of polydispersity.[20] The

dependence of the initial particle growth kinetics on the method of adding the reducing solution is dramatic: Figure 2 shows the average nanocrystal size increasing by only 15% during the first 2 h of the reaction (compared with a 100% increase in mean size for the first reaction method), and both the absolute standard deviation and standard deviation relative to the average radius remain nearly constant.

Late Stages of Nanocrystal Growth. At long times, nanocrystals can grow either by coagulation of the metal cores, condensation of monomer onto the nanocrystals, or a combination of both. The moments of the nanocrystal size distribution function, $\mu_1 = R_3/R_h$ and $\mu_3 = R_1/R_3$, reveal the relative contributions of condensation and coagulation to particle growth.[28,29] The arithmetic mean radius R_1 is defined as $\sum R_i/N_\infty$; R_3 is the cube-mean radius, given by $\sqrt[3]{\sum R_i^3/N_\infty}$; and R_h is the harmonic mean radius, defined as $N_\infty/\sum(1/R_i)$, where N_∞ is the total number of particles. For a monodisperse sample, $\mu_1 = \mu_3 = 1$ and values of $\mu_1 < 1.25$ and $\mu_3 > 0.905$ indicate that a condensation mechanism controls growth.[28] Since SAXS cannot be used to determine the *shape* of the size distribution, the nanocrystal size distribution functions were determined from TEM images of multiple samples using both reaction schemes. At least 250 particles were measured for each sample and the images used for analysis were taken from different areas of the TEM grid in all cases. For all of the samples examined, the average moments were $\mu_1 = 1.04$ and $\mu_3 = 0.98$, indicating that the nanocrystals grow primarily by condensation.

The rate of monomer condensation can be limited by either the molecular transport to the surface or the surface reaction rate of the adsorbed monomer. The size distribution evolves according to the rate-limiting step for particle growth.[30] For diffusion-controlled growth, conditions of high supersaturation give rise to a decreasing σ over the course of the reaction; whereas, low supersaturation leads to values of σ that increase with particle growth. For surface-reaction-controlled growth, σ does not depend on the supersaturation and remains constant during particle growth. Figure 2c shows that σ is nearly constant, varying less than 1.1 Å, over the course of the reaction. The sharpening of σ/R_{avg} in Figure 2b results from increased R_{avg} throughout the course of the reaction.

It is also straightforward to compare the characteristic times for mass transfer and surface reaction, τ_t and τ_r, respectively, by calculating the dimensionless Damköhler number: $Da = \tau_t/\tau_r = (a/k_L')/(1/k_r)$. The quantity a/k_L' is the characteristic reaction length a, taken as the ratio of the volume to surface area of the gold core $a = R/3$,[31] divided by the liquid-phase mass transfer coefficient k_L'. The characteristic reaction time is the reciprocal of the rate constant k_r. Using the mass transfer coefficient and rate constant calculated for this system, $k_L' = 3.4 \times 10^{-5}$ m/s and $k_r = 5.0 \times 10^{-5}$ s^{-1},[32] and taking R as the average radius of the nanocrystals at the end of the reaction ($R = 2.6$ nm), it was determined that $Da = 1.3 \times 10^{-9}$, indicating that nanocrystal growth at long times is limited by the surface reaction rate.

Nanocrystal Thermodynamics. Despite significant differences in initial precursor concentration and early time growth kinetics, remarkable agreement occurs in size and polydispersity after 24 h of particle growth. The existence of a thermodynamically stable (or metastable) size of gold nanocrystals has been suggested in experimental work by several researchers.[33−38] The theoretical framework, which is presented briefly here, has been dealt with in detail by Gelbart and co-workers[35,39] and Chikan and Kelley.[40]

The total free energy (per atom) of a collection of monodisperse nanocrystals with N total atoms in the system, $A_{total}(R)$, depends on the free energy contributions due to the surface tension and ligand binding: $A_{total}(R) = A_{surface}(R) + A_{TOAB}(R)$. Surface tension always favors particle growth, whereas ligand binding can favor smaller nanocrystals. Gold atoms in nanocrystals have a higher surface energy than in the bulk because of the interfacial curvature, and the surface free energy,

$$A_{surface}(R) = N\frac{3}{R}\mu(R)$$

can be expressed in terms of the size-dependent chemical potential given by the Gibbs−Thomson equation,

$$\mu(R) = \mu_{bulk} + \frac{2\,\gamma\,V_m}{R}$$

where γ is the surface free energy and V_m is the volume per atom of the bulk metal. $A_{surface}(R)$ can then be written in the form,

$$A_{surface}(R) = \frac{\alpha}{R} + \frac{\beta}{R^2}$$

where α and β are positive constants.[40,41] Gold atoms in smaller nanocrystals have a more positive free energy, making them thermodynamically less stable than larger particles. Ligand binding on the nanocrystal surface, on the other hand, tends to stabilize smaller nanocrystals, with the free energy contribution from the bound protective molecules having the form

$$A_{TOAB} = \frac{\zeta}{R}$$

where $\zeta < 0$ when ligand binding is energetically favorable.[35,40] The total free energy has the form

$$A_{total} = \frac{\alpha + \zeta}{R} + \frac{\beta}{R^2}$$

If $\alpha + \zeta < 0$, then a radius $R = -2\beta/(\alpha + \zeta)$ exists that minimizes the free energy and corresponds to a thermodynamically favorable size. In the present work, it appears that a favored size occurs for both reaction pathways after 24 h. However, the nanocrystals are not true equilibrium structures as they aggregate and eventually precipitate after several days of stirring. The TOAB does not bind strongly enough to stabilize the nanocrystals for exceedingly long times (i.e., days), whereas dispersions of nanocrystals coated with stronger binding agents have been observed to be stable for months or longer.[11]

The analysis above suggests that increased binding strength between the protective ligand and the gold surface (i.e., ζ becomes more negative) favors a smaller nanocrystal size. This is confirmed experimentally by varying the binding strength of the ligand present during growth. Gold nanocrystals were synthesized in the presence of a 20-fold excess of tetraoctylammonium bromide, tetraoctylphosphonium bromide, or a mixture of tetraoctylammonium bromide and octanethiol (in which the TOAB acts as the phase transfer catalyst and the more strongly binding thiol acts as the capping ligand during growth) and allowed to react for 24 h. The gold−ligand binding strength varies as amine < phosphine < thiol.[36] Figure 4 shows the results from each nanocrystal synthesis; as expected from the model, the particle size varies inversely with the binding strength of the capping ligand. SAXS measurements indicate that after

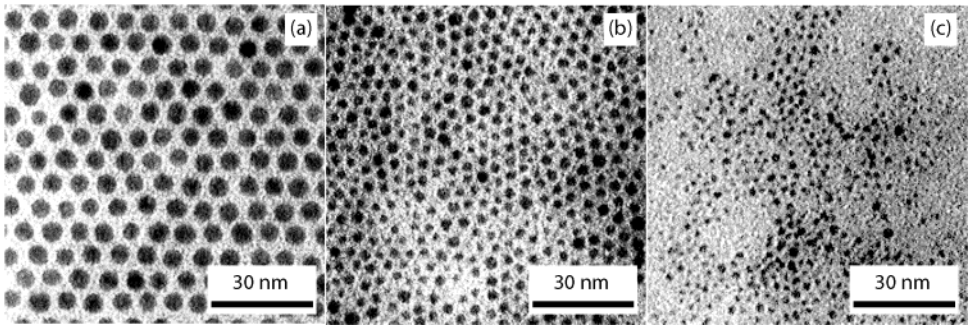

Figure 4. TEM images of nanocrystals stabilized with (a) tetraoctylammonium bromide, (b) tetraoctylphosphonium bromide, and (c) octanethiol during growth. The nanocrystals were allowed to react for 24 h before collection. The mean nanocrystal size decreases as the binding strength of the capping ligand increases, as is expected from the thermodynamic considerations discussed in the text.

24 h the average diameter of the tetraoctylammonium-capped particles is 5.3 ± 0.54 nm; for the tetraoctylphosphonium-capped particles the average diameter is 2.90 ± 0.67 nm; the octanethiol-capped particles had an average diameter of 1.7 ± 0.32 nm. After growth is complete the amine and phosphine stabilizers could be displaced from the surface by adding a more strongly binding thiol. In this manner the mean size of the resulting dispersion is easily controlled through appropriate choice of passivating agent during growth.

It is important to note that the sizes observed for the phosphine and thiol-capped nanocrystals may be smaller than the sizes which would be predicted from the free energy considerations discussed above. Although the final size is likely thermodynamically driven, the *rate* at which this size is achieved may also vary significantly with the ligand binding strength. The amine-passivated nanocrystals reach their final size within 24 h; observations of hexanethiol-coated gold nanoparticles, however, show a slow increase of the average size over a period of days.[42] Since the reactions were allowed to proceed for only 1 day, the measured size distributions may correspond to an intermediate state in which growth was halted through precipitation and cleaning of the nanocrystals. It has been demonstrated that nanocrystal capping ligands for a variety of systems are relatively labile and the surface coverage reaches an equilibrium with the surrounding medium.[14,15] In the studied systems, the capping ligand is present in large excess in the reaction solution, favoring high nanocrystal surface coverage; this, combined with the strong binding of the ligand to the surface, may provide increased steric repulsion which slows the mechanism for particle interaction and growth.

Conclusions

The growth of gold nanocrystals passivated with tetraoctylammonium bromide was examined using small-angle X-ray scattering to obtain accurate information about the evolution of the size and size distribution. For reaction times of less than a few hours, the growth kinetics depend on the initial concentration of gold precursor and the rate of addition of the reducing agent solution. The degree of supersaturation could be controlled in this manner, which influences whether the nucleation and growth stages occur independently or simultaneously. It was further found that the particle size and size distribution obtained after long reaction times are independent of the initial reaction kinetics. Analysis of the final particle size distribution and the rates of transport and reaction in the system indicate that at long reaction times the particle growth is limited by adsorption and reaction of the gold monomer onto the surface of the nanocrystals. It is suggested that the particle size at long times corresponds to a thermodynamically metastable state in which the system free energy contributions from the gold surface and the binding of the ligands reach a local minimum. The model predictions agree qualitatively with experimental results in which the strength of the binding ligand present during growth was varied. It was found that average particle size varies inversely with the ligand binding strength, allowing the mean diameter to be easily tuned between 1.7 and 5.2 nm. Such an analysis should be generally applicable to other reactions which are thermodynamically controlled and provide insight to particle size control.

Acknowledgment. This work is supported in part by the STC Program of the National Science Foundation under agreement No. CHE-9876674, the Welch Foundation, and the Texas Higher Education Coordinating Board through their ATP program.

References and Notes

(1) Hornyak, G. L.; Patrissi, C. J.; Oberhauser, E. B.; Martin, C. R.; Valmalette, J. C.; Lemaire, L.; Dutta, J.; Hofmann, H. *Nanostruct. Mater.* **1997**, *9*, 571.
(2) Faraday, M. *Philos. Trans. R. Soc. London* **1857**, *147*, 145.
(3) Mie, G. *Ann. Phys.* **1908**, *25*, 377.
(4) Zhong, C.-J.; Maye, M. M. *Adv. Mater.* **2001**, *13*, 1507.
(5) Kim, T. S.; Stiehl, J. D.; Reeves, C. T.; Meyer, R. J.; Mullins, C. B. *J. Am. Chem. Soc.* **2003**, *125*, 2018.
(6) Beesley, J. E. *Proc. R. Microsc. Soc.* **1985**, *20*, 187.
(7) Yu, H.; Gibbons, P. C.; Kelton, K. F.; Buhro, W. E. *J. Am. Chem. Soc.* **2001**, *123*, 9198.
(8) Lu, X.; Hanrath, T.; Johnston, K. P.; Korgel, B. A. *Nano Lett.* **2003**, *3*, 93.
(9) Hanrath, T.; Korgel, B. A. *Adv. Mater.* **2003**, *15*, 437.
(10) Brust, M.; Walker, M.; Bethell, D.; Schiffrin, D. J.; Whyman, R. *J. Chem. Soc., Chem. Commun.* **1994**, 801.
(11) Brust, M.; Fink, J.; Bethell, D.; Schiffrin, D. J.; Kiely, C. *J. Chem. Soc., Chem. Commun.* **1995**, 1655.
(12) *X-ray Characterization of Materials*; Lifshin, E., Ed.; Wiley-VCH: New York, 1999.
(13) Korgel, B. A.; Fitzmaurice, D. *Phys. Rev. B* **1999**, *59*, 14191.
(14) Mattoussi, H.; Cumming, A. W.; Murray, C. B.; Bawendi, M. G.; Ober, R. *Phys. Rev. B* **1998**, *58*, 7850.
(15) Korgel, B. A.; Fullam, S.; Connolly, S.; Fitzmaurice, D. *J. Phys. Chem. B* **1998**, *102*, 8379.
(16) Guinier, A.; Fournet, G. *Small-Angle Scattering of X-rays*; Wiley: New York, 1955.
(17) *Small-Angle X-ray Scattering*; Glatter, O.; Kratky, O., Eds.; Academic Press: New York, 1982.
(18) Whetten, R. L.; Shafigullin, M. N.; Khoury, J. T.; Schaaff, T. G.; Vezmar, I.; Alvarez, M. M.; Wilkinson, A. *Acc. Chem. Res.* **1999**, *32*, 397.
(19) La Mer, V. K.; Dinegar, R. H. *J. Am. Chem. Soc.* **1950**, *72*, 4847.
(20) LaMer, V. K. *J. Ind. Eng. Chem.* **1952**, *44*, 1270.
(21) Hyeon, T.; Lee, S. S.; Park, J.; Chung, Y.; Na, H. B. *J. Am. Chem. Soc.* **2001**, *123*, 12798.
(22) Peng, X.; Wickham, J.; Alivisatos, A. P. *J. Am. Chem. Soc.* **1998**, *120*, 5343.
(23) Peng, Z. A.; Peng, X. *J. Am. Chem. Soc.* **2002**, *124*, 3343.
(24) *Fine Particles: Synthesis, Characterization, and Mechanisms of Growth*; Sugimoto, T., Ed.; Marcel Dekker: New York, 2000; Vol. 92.

(25) Thomas, K. G.; Zajicek, J.; Kamat, P. V. *Langmuir* **2002**, *18*, 3722.
(26) Fink, J.; Kiely, C. J.; Bethell, D.; Schiffrin, D. J. *Chem. Mater.* **1998**, *10*, 922.
(27) Sugimoto, T. *Adv. Colloid Interface Sci.* **1987**, 28.
(28) Pich, J.; Friedlander, S. K.; Lai, F. S. *J. Aerosol Sci.* **1970**, *1*, 115.
(29) Shah, P. S.; Husain, S.; Johnston, K. P.; Korgel, B. A. *J. Phys. Chem. B* **2001**, *105*, 9433.
(30) Sugimoto, T. *Monodispersed Particles*, 1st ed.; Elsevier: New York, 2001.
(31) Rawlings, J. B.; Ekerdt, J. G. *Chemical Reactor Analysis and Design Fundamentals*; Nob Hill Publishing: Madison, WI, 2002.
(32) The term k_L' was estimated from the mass transfer correlation for a dilute, vigorously stirred system:[41]

$$k_L' = 0.13 N_{Sc}^{-2/3} \left[\frac{(P/V_{\tan k})\mu_L}{\rho_L^2} \right]^{1/4} \quad (3)$$

The parameters necessary for the calculation are the Schmidt number, $N_{Sc} = (\mu_L/\rho_L D_{AB})$, the power transferred to the fluid from the stir bar P, the liquid volume V_{tank}, and the viscosity and density of the liquid phase (toluene) μ_L and ρ_L. The diffusion coefficient D_{AB} of the gold−tetraoctylammonium bromide complex in toluene is calculated using the Stokes−Einstein equation, $D_{AB} = kT/\mu_L 6\pi R_c = 3.3 \times 10^{-10}$ m^2/s (where k is Boltzmann's constant, T is the solvent temperature, and R_c is the radius of the gold complex, taken as the length of a fully extended TOAB molecule, approximately 1.2 nm).[13] The maximum power input to the fluid from the stir bar is calculated to be 0.1 W.[41] Using these values and eq 3, we find that $k_L' = 3.4 \times 10^{-5}$ m/s. The term k_r can be determined from the time-dependent growth data (Figure 2) by examining the depletion rate of the gold monomer concentration $dC_{Au}/dt = -k_r C_{Au}^n$. The reaction order, n, was assessed by plotting the appropriate form of the integrated rate equation against C_{Au}. C_{Au} was estimated by assuming a constant number of nanocrystals at long reaction time, taking the nanocrystal diameter as the ensemble average measured using SAXS and assuming complete conversion of gold monomer to nanocrystals at long reaction times. Several reaction orders were considered and it was found that the data was best described by first-order kinetics. For $n = 1$, the integrated rate equation is $\ln(C_{Au}/C_{Au,0}) = -k_r t$, where $C_{Au,0}$ is the initial concentration of gold in the system. The time-dependent concentration data is plotted in this form, and the slope of the data for reaction times greater than 4 h yielded $k_r = 5.0 \times 10^{-5}$ s^{-1} for both reaction methods.

(33) Maye, M. M.; Zheng, W.; Leibowitz, F. L.; Ly, N. K.; Zhong, C.-J. *Langmuir* **2000**, *16*, 490.
(34) Teranishi, T.; Hasegawa, S.; Shimizu, T.; Miyake, M. *Adv. Mater.* **2001**, *13*, 1699.
(35) Leff, D. V.; Ohara, P. C.; Heath, J. R.; Gelbart, W. M. *J. Phys. Chem.* **1995**, *99*, 7036.
(36) Prasad, B. L. V.; Stoeva, S. I.; Sorensen, C. M.; Klabunde, K. J. *Chem. Mater.* **2003**, *15*, 935.
(37) Prasad, B. L. V.; Stoeva, S. I.; Sorensen, C. M.; Klabunde, K. J. *Langmuir* **2002**, *18*, 7515.
(38) Lin, X. M.; Sorensen, C. M.; Klabunde, K. J. *J. Nanopart. Res.* **2000**, *2*, 157.
(39) Whetten, R. L.; Gelbart, W. M. *J. Phys. Chem.* **1994**, *98*, 3544.
(40) Chikan, V.; Kelley, D. F. *J. Phys. Chem. B* **2002**, *106*, 3794.
(41) *Perry's Chemical Engineers' Handbook*; 7th ed.; Perry, R. H., Green, D. W., Eds.; McGraw-Hill: New York, 1998.
(42) Chen, S.; Templeton, A. C.; Murray, R. W. *Langmuir* **2000**, *16*, 3543.